



Beclin1-driven autophagy modulates the inflammatory response of microglia via NLRP3

Judith Houtman¹, Kiara Freitag^{1,2}, Niclas Gimber³, Jan Schmoranzer³ , Frank L Heppner^{1,2,4,†} & Marina Jendrach^{1,*} 

Abstract

Alzheimer's disease is characterized not only by extracellular amyloid plaques and neurofibrillary tangles, but also by microglia-mediated neuroinflammation. Recently, autophagy has been linked to the regulation of the inflammatory response. Thus, we investigated how an impairment of autophagy mediated by BECN1/Beclin1 reduction, as described in Alzheimer's disease patients, would influence cytokine production of microglia. Acutely stimulated microglia from *Becn1*^{+/-} mice exhibited increased expression of IL-1beta and IL-18 compared to wild-type microglia. *Becn1*^{+/-} *APPSP1* mice also contained enhanced IL-1beta levels. The investigation of the IL-1beta/IL-18 processing pathway showed an elevated number of cells with inflammasomes and increased levels of NLRP3 and cleaved CASP1/Caspase1 in *Becn1*^{+/-} microglia. Super-resolution microscopy revealed a very close association of NLRP3 aggregates and LC3-positive vesicles. Interestingly, CALCOCO2 colocalized with NLRP3 and its downregulation increased IL-1beta release. These data support the notion that selective autophagy can impact microglia activation by modulating IL-1beta and IL-18 production via NLRP3 degradation and thus present a mechanism how impaired autophagy could contribute to neuroinflammation in Alzheimer's disease.

Keywords Alzheimer's disease; autophagy; BECN1/Beclin1; inflammation; microglia

Subject Categories Immunology; Neuroscience

DOI 10.15252/embj.201899430 | Received 15 March 2018 | Revised 28

November 2018 | Accepted 5 December 2018 | Published online 7 January 2019

The EMBO Journal (2019) 38: e99430

Introduction

Alzheimer's disease (AD) is the most common neurodegenerative disorder. The main hallmarks of AD are extracellular amyloid

plaques (main component amyloid-beta (Aβ) peptide), neurofibrillary tangles (the main component hyperphosphorylated MAP tau), and neuroinflammation. Microglia, the resident immune cells of the central nervous system, are involved in two aspects of AD: removal of extracellular Aβ by phagocytosis and production and release of cytokines resulting in progressive neuroinflammation. Neuroinflammation correlates in many animal models with an increase in extracellular Aβ, and microglia are regarded as the main producers of pro-inflammatory cytokines (Heppner *et al*, 2015). *In vivo* interleukin (IL)-1 (Griffin *et al*, 1989), IL-6, granulocyte-macrophage colony-stimulating factor (GM-CSF) (Patel *et al*, 2005), IL-12, and IL-23 (Vom Berg *et al*, 2012), as well as tumor necrosis factor (TNF) alpha (Fillit *et al*, 1991), were detected in human patients with AD or in different animal models with AD-like pathology (Prokop *et al*, 2013). While enhanced neuroinflammation is well established in the late stages of AD, recent data also suggest a role for inflammation in the development of the disease. Injection of double-stranded RNA (Poly:IC) into wild-type mice, thus mimicking viral infection, resulted in increased IL-1beta levels followed by an AD-like pathology at higher age (Krstic *et al*, 2012). Furthermore, mouse models lacking the pro-IL-1beta processing proteins NLRP3 (NLR family, pyrin domain containing 3) or CASP1/Caspase1 show decreased inflammation and Aβ burden and increased Aβ phagocytosis (Heneka *et al*, 2013).

The mechanisms behind enhanced microglial activation and increased cytokine release in AD seem to be diverse. Priming of microglia by interaction with Aβ is a possibility (Heppner *et al*, 2015). Another or additional mechanism could be autophagy, as recent work on myeloid cells indicates that impaired autophagy mediates increased inflammation. Mutations in the AD risk factor TREM2 are linked to anomalous autophagy (Ulland *et al*, 2017). Loss of the autophagy protein ATG16L1 is associated with Crohn's disease and resulted in enhanced pro-inflammatory cytokine production of macrophages in response to stress (Saitoh *et al*, 2008; Murthy *et al*, 2014). A conditional knock-out of *Atg5* or *Atg7* in macrophages correlated with increased severity of uveitis (Santeford

1 Department of Neuropathology, Charité – Universitätsmedizin Berlin, corporate member of Freie Universität Berlin, Humboldt-Universität zu Berlin, Berlin Institute of Health, Berlin, Germany
 2 German Center for Neurodegenerative Diseases (DZNE) within the Helmholtz Association, Berlin, Germany
 3 Core Facility Advanced Medical Bioimaging (AMBIO), Charité – Universitätsmedizin Berlin, corporate member of Freie Universität Berlin, Humboldt-Universität zu Berlin, Berlin Institute of Health, Berlin, Germany
 4 Cluster of Excellence, NeuroCure, Berlin, Germany
 *Corresponding author. Tel: +49 30 450536291; E-mail: marina.jendrach@charite.de
 †These authors contributed equally to this work

et al, 2016), liver fibrosis (Lodder et al, 2015), or colitis (Lee et al, 2016). *In vitro* data on macrophages and macrophage cell lines show that addition of the autophagy blocker 3-MA resulted in increased IL-1 β formation (Harris et al, 2011; Zhou et al, 2011; Shi et al, 2012; de Luca et al, 2014). Data on microglia are emerging but are somewhat controversial: Some publications describe increased activation of primary mouse microglia or the microglial cell line BV2 after knockdown of autophagy genes (Cho et al, 2014; Ye et al, 2017) or lysosomal damage by manganese (Wang et al, 2017). Others have reported no changes in cytokine release when autophagic flux was blocked for 24 h by Bafilomycin A1 (François et al, 2013).

Microglia isolated from human AD patients show strongly reduced protein levels of BECN1/Beclin1 (Lucin et al, 2013). BECN1 is an essential part of the multi-protein complex that is necessary for nucleation of the autophagic vesicle (Zhang et al, 2016). Homozygous loss of *Becn1* causes embryonic cell death between E7.5 and E8.5 (Yue et al, 2003), while heterozygous loss of *Becn1* mediates decreased autophagy in different cell types (Qu et al, 2003; Pickford et al, 2008). Furthermore, heterozygous loss of *Becn1* in an AD mouse model (T41 *APP*^{+/-} mice) resulted in increased A β burden (Pickford et al, 2008). In addition, BECN1 was shown to be involved in receptor recycling and retromer recruitment in phagocytosis of A β *in vitro* (Lucin et al, 2013).

Based on these data, we envision a central role for microglial BECN1 in the regulation of neuroinflammation.

Results

Reduction in BECN1 and impairment of autophagy results in enhanced IL-1 β and IL-18 release from microglia

To investigate whether modulation of BECN1 levels in microglia influences neuroinflammatory responses, *Becn1*^{+/-} mice were chosen as a model system with reduced BECN1 levels. The use of *Becn1* heterozygous mice was necessary since *Becn1*^{-/-} mice die *in utero* before the microglia precursor cells leave the yolk sac to colonize the developing brain (Yue et al, 2003). Microglia were isolated from newborn *Becn1*^{+/-} and wild-type mouse pups. The BECN1 content of microglia from *Becn1*^{+/-} and wild-type mice was assessed by Western blotting: Microglia from *Becn1*^{+/-} mice show around 50% reduction in BECN1 protein compared to microglia from wild-type mice (Fig 1A). Next, the effect of BECN1 reduction

on autophagy was determined. Microglia were kept for 2 h either in cultivation medium (DMEM with 10% FCS) or in amino acid-free starvation medium (HBSS), in the presence or absence of Bafilomycin A1. While the HBSS-cultured microglia showed a trend of decreased autophagic flux in the Bafilomycin A1-treated *Becn1*^{+/-} microglia, LC3-II/MAP1LC3B-II levels of *Becn1*^{+/-} microglia were significantly lower when autophagic flux was blocked with Bafilomycin A1 in medium-exposed cells, in accordance with the reduced BECN1 content (Fig 1B). Staining of endogenous LC3-positive vesicles in Bafilomycin A1-treated microglia supports these data (Fig 1C).

To determine the effect of BECN1 and autophagy reduction on inflammation, microglia were treated with a standard acute pro-inflammatory stimulus: Cells were subjected for 3 h to LPS (1 μ g/ml) followed by 45 min of ATP (1 mM). To quantify the release of pro-inflammatory cytokines, AD-relevant cytokines IL-1 β , IL-18, TNF α , and IL-6 were measured by ELISA. Reduction in BECN1 resulted in an increased presence of IL-1 β and IL-18 in the supernatant of LPS/ATP-stimulated *Becn1*^{+/-} microglia compared to the supernatant of LPS/ATP-stimulated wild-type microglia (Fig 2A and B). Increased IL-1 β levels were also detected in the supernatant of *Becn1*^{+/-} microglia by Western blot (Fig EV1A). In contrast, levels of TNF α and IL-6 were not altered (Fig EV1B).

Subsequently, we sought to confirm these data by a pharmacological approach: Microglia isolated from wild-type mouse pups were treated with the pro-inflammatory stimulus in growth medium with 10% FCS or in amino acid-free starvation medium HBSS. IL-1 β release after stimulation with LPS/ATP was significantly lower in cells kept in HBSS (Fig 2C). Furthermore, wild-type microglia in full medium or HBSS were stimulated with LPS and ATP in the presence or absence of the autophagy blocker 3-Methyladenine (3-MA). Short-term treatment of 3-MA for 1 h 45 min resulted in reduction in LC3-positive vesicles (Fig 2D) and in a significant increase in IL-1 β (Fig 2C). While cells kept in HBSS released less cytokines in general, TNF α release was decreased upon 3-MA treatment in growth medium as well as in HBSS medium, whereas the IL-6 release was not affected by 3-MA treatment (Fig EV1C).

To investigate whether reduced BECN1 levels also have an effect on inflammation *in vivo*, we crossed *Becn1*^{+/-} mice to *APP*^{PS1} mice. *APP*^{PS1} mice are an established AD model with progressive amyloid-beta pathology and corresponding neuroinflammation (Radde et al, 2006). *APP*^{PS1} *Becn1*^{+/-} mice were analyzed at 3 months (amyloid-beta deposits detectable in the brain), 4 months

Figure 1. Autophagy is impaired in *Becn1*^{+/-} microglia.

- A BECN1 expression of microglia from *Becn1*^{+/-} and wild-type mouse pups in full medium without Bafilomycin A1 (Baf) was quantified by Western blotting. Microglia from *Becn1*^{+/-} mice show a significant reduction in BECN1 (48%) compared to microglia from wild-type mice; mean \pm SEM, wild-type $n = 3$, *Becn1*^{+/-} $n = 7$; two-tailed t -test $**P < 0.01$. Blot shows representative amounts of BECN1 after various treatments.
- B Microglia from newborn *Becn1*^{+/-} and wild-type mouse pups were kept for 2 h either in full medium or in HBSS with or without Bafilomycin A1 (Baf). LC3 and ACTIN levels were determined by Western blot. LC3-II was significantly reduced in microglia from *Becn1*^{+/-} mice after Baf treatment in full medium compared to wild-type microglia; mean \pm SEM, wild-type $n = 3$, *Becn1*^{+/-} $n = 4$; two-tailed t -test $*P < 0.05$.
- C Microglia from newborn *Becn1*^{+/-} and wild-type mouse pups were kept for 2 h either in full medium or HBSS with Bafilomycin A1 (Baf) and stained for endogenous LC3. Exemplary images and the quantification of LC3-positive vesicles/ μ m² cell area show reduced presence of LC3-positive vesicles in microglia from *Becn1*^{+/-} mice and induction of autophagy by HBSS; mean \pm SEM, wild-type $n = 4$, *Becn1*^{+/-} $n = 4$, 3–5 fields per view/ n and condition and 73–271 cells/ n and condition; two-tailed t -test $*P < 0.05$; scale bar: 20 μ m.

Source data are available online for this figure.

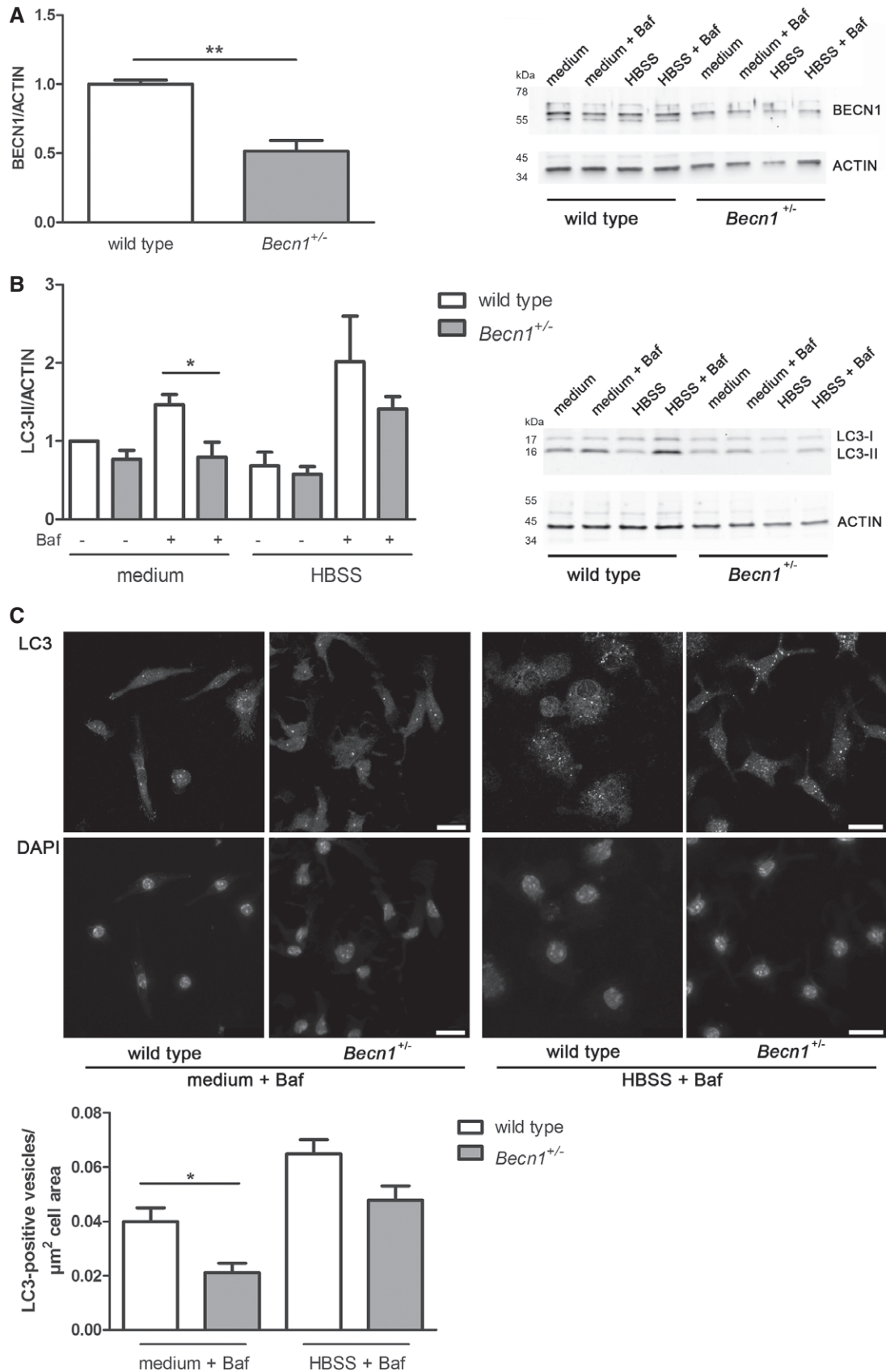


Figure 1.

Figure 2. Reduction in BECN1 results in enhanced IL-1beta and IL-18 release.

- A, B Microglia isolated from newborn *Becn1*^{+/-} and wild-type mouse pups were either non treated or treated with a pro-inflammatory stimulus (LPS followed by ATP). As additional controls, cells treated only with LPS or ATP were used in (A). The concentration of the pro-inflammatory cytokines IL-1beta (A) and IL-18 (B) in the cell supernatant was determined by ELISA. Reduction in BECN1 significantly enhanced release of both cytokines after stimulation with LPS/ATP; mean ± SEM, wild-type *n* (A/B) = 9/2, wild-type LPS *n* = 3/0, wild-type ATP *n* = 3/0, wild-type LPS/ATP *n* = 9/9, *Becn1*^{+/-} *n* = 23/5, *Becn1*^{+/-} LPS/ATP *n* = 23/23, two-tailed *t*-test **P* < 0.05.
- C Microglia isolated from wild-type mouse pups were pre-incubated in full medium or starvation medium HBSS before addition of a pro-inflammatory stimulus (LPS followed by ATP). The autophagy blocker 3-MA was added for the final 1 h 45 min of the experiment. The concentration of the pro-inflammatory cytokine IL-1beta in the cell supernatant was determined by ELISA. Incubation with HBSS reduced IL-1beta release significantly while 3-MA treatment increased it; mean ± SEM, full medium *n* = 6, full medium LPS/ATP *n* = 6, full medium LPS/ATP + 3-MA *n* = 3, HBSS *n* = 6, HBSS LPS/ATP *n* = 6, HBSS LPS/ATP + 3-MA *n* = 6; two-tailed *t*-test **P* < 0.05; ***P* < 0.01.
- D Microglia isolated from wild-type mouse pups were pre-incubated in starvation medium HBSS before addition of a pro-inflammatory stimulus (LPS followed by ATP). The autophagy blocker 3-MA was added for the final 1 h 45 min of the experiment, microglia were stained for LC3, and images were taken by confocal microscopy. Representative images show a reduction in LC3-positive vesicles in 3-MA-treated cells. Scale bar: 20 μm.
- E Proteins were extracted from brains of wild-type, *Becn1*^{+/-}, *APPPS1*, and *APPPS1 Becn1*^{+/-} mice at the indicated ages. IL-1beta was measured by electrochemiluminescence (Meso Scale) and compared within the respective age groups. IL-1beta was significantly increased in the TBS and TX fraction; mean ± SEM, wild-type: *n* (per age group) = 2/6/3, *Becn1*^{+/-}: *n* = 2/5/2, *APPPS1*: *n* = 5/5/6, *APPPS1 Becn1*^{+/-}: *n* = 7/9/6; ANOVA with Dunnett's *post hoc* test with WT as control group; **P* < 0.05; ***P* < 0.01.
- F Proteins were extracted from brains of *APPPS1* and of *APPPS1 Becn1*^{+/-} mice at the indicated ages. Amyloid-beta 1-40 and 1-42 were measured by electrochemiluminescence (Meso Scale) and compared within the respective age groups. No difference in the amyloid-beta load between the genotypes is apparent; mean ± SEM, *APPPS1*: *n* = 5/5/6, *APPPS1 Becn1*^{+/-}: *n* = 7/9/6; ANOVA with Dunnett's *post hoc* test with *APPPS1* as control group, ns.

(plaque formation), and 8 months (full plaque pathology and cognitive deficits) and compared to age-matched wild-type, *Becn1*^{+/-} and *APPPS1* mice. The brains were processed in different buffers, resulting in four fractions containing proteins with different solubility (Kawarabayashi *et al*, 2001). The content of pro-inflammatory cytokines in the fractions containing highly soluble proteins (TBS and TX fraction) was analyzed by electrochemiluminescence (Meso Scale). While 3-month-old mice showed similar levels of IL-1beta regardless of the genotype, brain lysates of 4- and 8-month-old *APPPS1 Becn1*^{+/-} mice contained significantly more IL-1beta in both fractions (Fig 2E). In contrast, TNFalpha was not altered at all and IL-6 was only increased in the TX fraction but not the TBS fraction of 8-month-old *APPPS1 Becn1*^{+/-} mice (Fig EV1D and E).

To determine whether an increase in IL-1beta expression in *APPPS1 Becn1*^{+/-} mice may affect amyloid-beta pathology, we quantified the amount of amyloid-beta 1-40 and amyloid-beta 1-42 in protein lysates of brains from age-matched *APPPS1* and *APPPS1 Becn1*^{+/-} 3-, 4-, and 8-month-old mice by means of Meso Scale (Fig 2F) as well as by morphometric analyses of immunostained histological sections from brains of 4-month-old mice (Fig EV2A–C). Since we were not able to detect a significant difference in amyloid burden as well as in plaque size and plaque distribution in *APPPS1* versus *APPPS1 Becn1*^{+/-} mice (Figs 2F and EV2A–C), we compared the phagocytic capacity of microglia in acute brain slices from 4-month-old *Becn1*^{+/-} mice to those of microglia from wild-type mice. Again, no significant differences with respect to the amount of phagocytic cells or the overall phagocytic index became apparent (Fig EV2D–F). Taken together, these data demonstrate that reducing BECN1 and, thus, a diminution in autophagy increased specifically the release of IL-1beta and IL-18 from acute activated (LPS/ATP) and primed (amyloid-beta) microglia *in vitro* and *in vivo*, but did not substantially alter amyloid-beta pathology or phagocytosis *in vivo*.

Reduction in BECN1 influences the IL-1beta and IL-18 processing pathway

In order to assess the mechanism by which BECN1 is influencing IL-1beta and IL-18 production and/or release, we investigated the

crucial steps in the common pathway of IL-1beta and IL-18 production. The pro-inflammatory response starts with transcription and translation of the IL-1beta and IL-18 precursors followed by their processing at the inflammasome (Walsh *et al*, 2014). Therefore, microglia isolated from newborn *Becn1*^{+/-} and wild-type mouse pups were stimulated with LPS and ATP and the levels of pro-IL-1beta protein were determined by Western blotting. No differences in the levels of pro-IL-1beta were discernible (Fig EV3A).

Subsequently, the formation and assembly of the inflammasome, the protein complex responsible for processing pro-IL-1beta to IL-1beta by CASP1, were analyzed. The protein levels of NLRP3, the sensor component of the inflammasome, were analyzed by Western blotting in *Becn1*^{+/-} and wild-type microglia. While non treated cells expressed only low levels of NLRP3, stimulation with LPS/ATP increased NLRP3 expression strongly and activated microglia of *Becn1*^{+/-} mice contained significantly more NLRP3 than microglia of wild-type mice (Fig 3A). In contrast, no difference between the *Nlrp3* mRNA levels of *Becn1*^{+/-} and wild-type microglia was apparent (Fig 3B).

Next, inflammasome assembly was investigated by staining of ASC (apoptosis-associated speck-like protein containing a carboxy-terminal CARD), the adaptor protein for pro-CASP1 binding and processing. Again, microglia isolated from newborn *Becn1*^{+/-} and wild-type mouse pups were stimulated with LPS and ATP or left untreated. In non treated cells, ASC showed diffuse staining in the cytoplasm (Fig 3C). However, after stimulation, formation of inflammasomes could be observed in a subpopulation of cells, as well as release of inflammasomes after pyroptosis/ejection (Baroja-Mazo *et al*, 2014; Franklin *et al*, 2014). Quantification of these ASC foci in stimulated cells showed an almost threefold increased presence of inflammasomes in or around *Becn1*^{+/-} microglia (Fig 3C).

Finally, pro-CASP1 as substrate for the inflammasome and the processed, active CASP1 was analyzed. Pro-CASP1 protein levels in cell lysates of LPS/ATP-stimulated microglia showed no difference between *Becn1*^{+/-} and wild-type cells (Fig EV3B). However, Western blotting of the cell supernatant from stimulated microglia revealed that a significantly higher amount of cleaved, active CASP1 p10 was released from *Becn1*^{+/-} microglia compared to wild-type

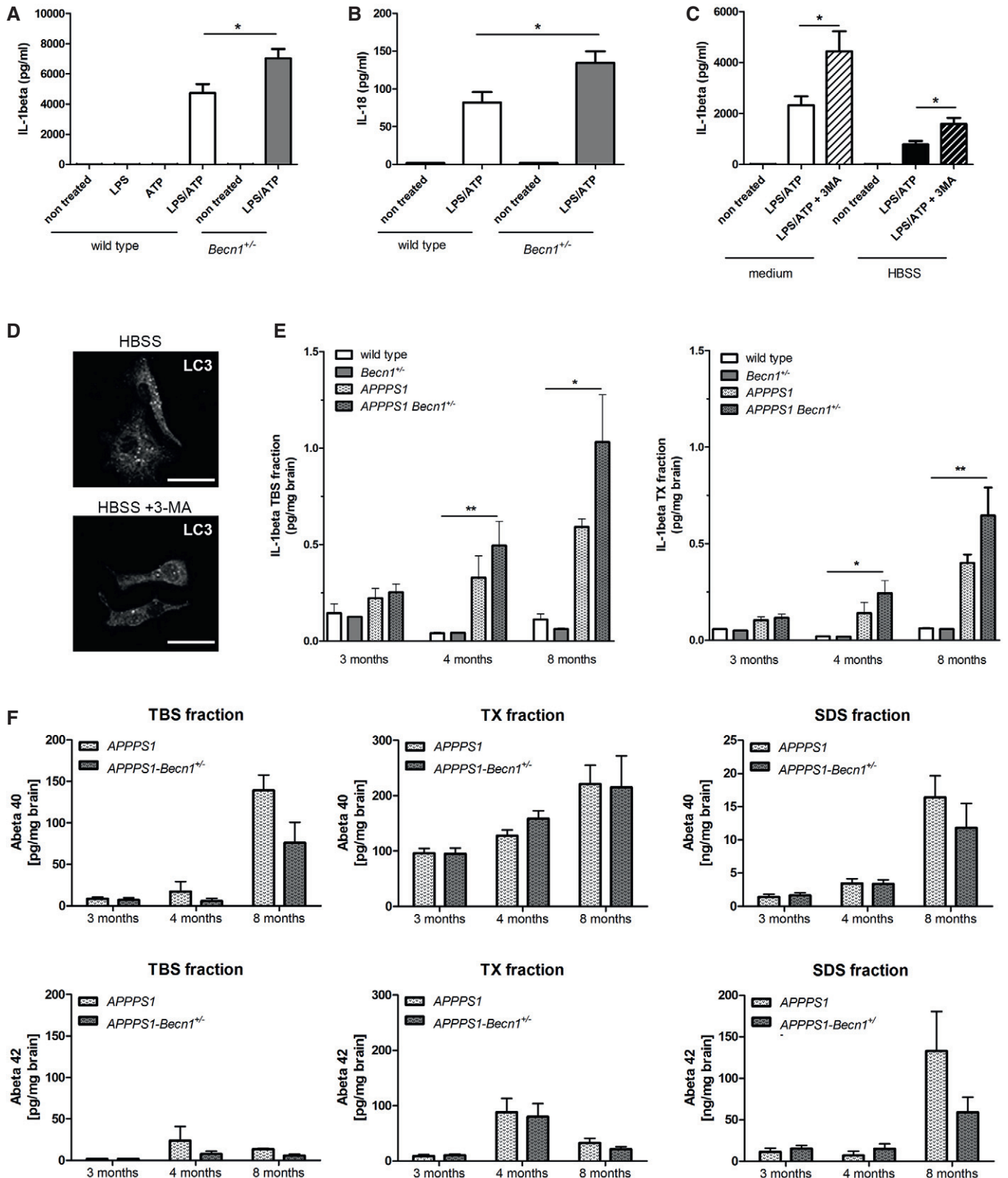


Figure 2.

microglia (Fig 3D). In addition, 3-MA treatment of wild-type microglia significantly increased the CASP1 p10 levels in the cell supernatant (Fig EV3C).

Taken together, these data indicate that the increase in IL-1beta and IL-18 production in *Becn1*^{+/-} microglia is linked to an upregulation of inflammasome formation and/or slower turnover.

NLRP3 is a substrate for autophagy

To determine the molecular mechanism of the effects described above, we assessed in detail how reduced BECN1 could mediate the observed increase in NLRP3 and inflammasomes in *Becn1*^{+/-} microglia. To obtain a comprehensive impression of NLRP3 appearance, and spatial distribution, endogenous NLRP3 was analyzed by immunocytochemistry. Non treated microglia showed, in correlation to their weak band in the Western blot, a diffuse cytoplasmic

staining with a few small NLRP3 puncta (Fig 4A). Stimulation of microglia with LPS/ATP resulted in the emergence of more and larger NLRP3 puncta/specs of different sizes (Fig 4A, arrows), indicating formation of NLRP3 oligomers or aggregates (Susjan et al, 2017) (see also Discussion). Quantification of NLRP3 aggregates in *Becn1*^{+/-} and wild-type microglia showed a higher number of NLRP3 aggregates in *Becn1*^{+/-} microglia (Fig EV4A). These data are in agreement with the NLRP3 protein levels quantified by Western blotting (Fig 3A). The subcellular localization as

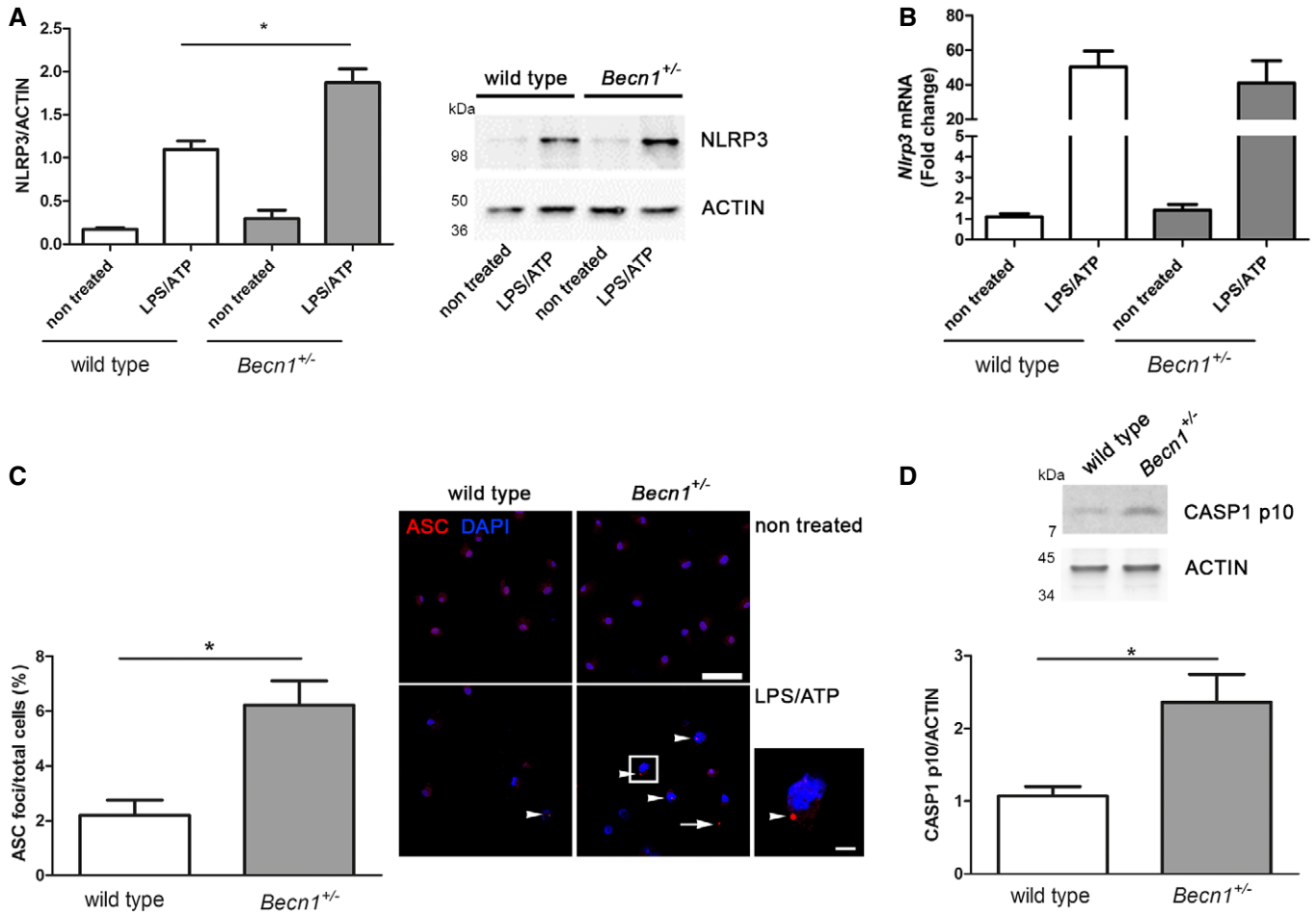


Figure 3. Reduction in BECN1 influences the IL-1beta processing pathway.

- A The expression of NLRP3 protein in non treated and LPS/ATP-treated wild-type and *Becn1*^{+/-} microglia was determined by Western blot and normalized to ACTIN. Reduction in BECN1 significantly enhanced expression of NLRP3; mean ± SEM, wild-type n = 4, wild-type LPS/ATP n = 9, *Becn1*^{+/-} n = 4, *Becn1*^{+/-} LPS/ATP n = 23; ANOVA with Tukey's post hoc test *P < 0.05.
- B The expression of *Nlrp3* mRNA in non treated and LPS/ATP-treated wild-type and *Becn1*^{+/-} microglia was determined by qPCR. No significant differences can be detected between wild-type and *Becn1*^{+/-} microglia; mean ± SEM, wild-type: n = 7, *Becn1*^{+/-}: n = 3; ANOVA with Tukey's post hoc test, ns for LPS/ATP-treated wild-type versus *Becn1*^{+/-}.
- C LPS/ATP-treated and non treated wild-type and *Becn1*^{+/-} microglia were immunolabeled for ASC (red) and imaged by confocal microscopy to investigate the assembly of inflammasomes. In non-stimulated cells, ASC is distributed diffusely in the cytoplasm (upper panels). However, after stimulation, formation of inflammasomes (arrowheads) can be detected in a subpopulation of cells as well as release of inflammasomes after pyroptosis/ejection (arrow). Quantification showed a significantly increased percentage of inflammasomes in or around *Becn1*^{+/-} microglia; mean ± SEM, wild-type LPS/ATP n = 4, *Becn1*^{+/-} LPS/ATP n = 7; two-tailed t-test *P < 0.05; scale bar: 50 μm, insert scale bar: 10 μm.
- D The presence of cleaved CASP1 (p10) protein in the supernatant of LPS/ATP-treated wild-type and *Becn1*^{+/-} microglia was determined by Western blot and normalized to ACTIN. Reduction in BECN1 significantly enhanced release of CASP1; mean ± SEM, wild-type LPS/ATP n = 8, *Becn1*^{+/-} LPS/ATP n = 18; two-tailed t-test *P < 0.05.

Source data are available online for this figure.

Figure 4. NLRP3 and LC3-positive vesicles are closely associated.

- A LPS/ATP-treated and non treated wild-type and *Becn1*^{+/-} microglia were immunolabeled for NLRP3 (green) and LC3 (red) and imaged by confocal microscopy. Stimulation resulted in the appearance of many NLRP3-containing aggregates of different sizes (arrows). In non treated cells, only a few overlapping signals with LC3-stained autophagosomes (arrowheads) are visible. Stimulated microglia, however, showed multiple colocalizations of LC3-positive vesicles and NLRP3 aggregates; scale bar: 7.5 μ m.
- B LPS/ATP-treated wild-type microglia were immunolabeled for NLRP3 (green) and LC3 (red) and analyzed by super-resolution microscopy (SIM). NLRP3 aggregates of different sizes coclustering with LC3-positive autophagosomes are clearly visible. 3D volume rendering of large (I) and small (II) NLRP3 aggregates from the magnified ROIs showed engulfment of NLRP3 by autophagosomes; scale bar: 10 μ m; magnified ROIs: 1 μ m.
- C 3D radial intensity profiles of NLRP3 and LC3 signals derived from SIM images in wild-type microglia, centered on the maxima of NLRP3 clusters. The radial profiles confirm that both proteins colocalize to the same organelle; mean \pm SEM, *n* = 4.

determined by the 3-dimensional distance of NLRP3 aggregates to the nucleus did not differ between *Becn1*^{+/-} and wild-type microglia (Fig EV4B). To confirm the specificity of the NLRP3 staining, stimulated microglia were co-labeled with ASC. As described previously (Walsh *et al*, 2014), we observed a very close association and partial overlap of NLRP3 and ASC signals using confocal and super-resolution microscopy (Fig EV4C and D).

To investigate the fate of the NLRP3 puncta/aggregates, microglia from *Becn1*^{+/-} and wild-type mouse pups were treated with LPS and ATP (alongside non treated controls) and then stained for endogenous NLRP3 and LC3. Confocal microscopy of non treated cells showed only a few overlapping signals of LC3-stained vesicles (arrowheads) and small NLRP3 puncta (arrows) (Fig 4A). However, stimulated microglia contained many LC3-positive vesicles that strongly colocalized with NLRP3 aggregates of different sizes (Fig 4A). These colocalizations appeared in both *Becn1*^{+/-} and wild-type microglia, indicating engulfment and probable degradation of NLRP3 by autophagosomes. As NLRP3 has been shown to colocalize with mitochondria (Zhou *et al*, 2011; Subramanian *et al*, 2013; Bracey *et al*, 2014), the localization of MTR-stained mitochondria, NLRP3, and LC3 was determined by confocal microscopy of LPS/ATP-stimulated cells. NLRP3 was found to colocalize not only with LC3, but also with MTR-stained mitochondria, and NLRP3 aggregates/puncta were in addition detectable in close vicinity to mitochondria though not directly colocalizing. A colocalization of NLRP3, LC3, and mitochondria was, however, not observed (Fig EV4E).

To gain a deeper understanding of the interaction of NLRP3 and autophagosomes, we performed 3D structured illumination microscopy (SIM), a super-resolution microscopy method that increases the conventional spatial resolution (i.e., confocal) by factor 2 in all three dimensions. SIM and subsequent 3D volume rendering of large (I) and small (II) NLRP3 aggregates showed indeed that LC3-positive structures corral around and partially overlap with the NLRP3 clusters in wild-type (Fig 4B) and *Becn1*^{+/-} microglia (Appendix Fig S1A, see also Appendix videos of 3D projections). In order to confirm that NLRP3 clusters really present a substrate for autophagy, we quantified the colocalization of NLRP3 and LC3 by performing 3D radial intensity profiles around the center of NLRP3 clusters (Figs 4C and 5D). Indeed, both proteins colocalized to the same organelle as indicated by an overlap of both maxima in the radial intensity profile. The signal decay within the known size of autophagosomes (Mizushima *et al*, 2002) indicates that NLRP3 aggregates were indeed engulfed/taken up by the LC3-positive vesicles (Fig 4C, Appendix Fig S1B and C).

To assess whether NLRP3 aggregates exist also in microglia of adult mice, an *ex vivo* approach was employed: Microglia were isolated from 8-month-old wild-type and *APPPS1* mice and cultivated for 4 h. Subsequent confocal microscopy revealed NLRP3

aggregates as well as LC3-positive vesicles inside these cells. Furthermore, some NLRP3 signals colocalized with LC3, further supporting the conclusion that NLRP3 degradation occurs through autophagy (Fig EV5A). In contrast to microglia, neonatal murine astrocytes as yet another cytokine-producing brain cell did not contain NLRP3 (Fig EV5B and C).

CALCOCO2/NDP52 colocalizes with NLRP3 and modulates IL-1beta release

In order to determine the interaction between NLRP3 and the vesicles on the molecular level, we investigated possible adaptor proteins. p62/SQSTM1 has been described as an adaptor protein for the autophagic removal of inflammasomes (Shi *et al*, 2012). Therefore, we stained NLRP3 and p62 in LPS/ATP-treated but detected no colocalization (Appendix Fig S2A). In contrast, CALCOCO2/NDP52 (arrowheads) which acts as an autophagic adaptor protein in human cells colocalized with smaller and larger NLRP3 aggregates (arrows) in LPS/ATP stimulated wild-type microglia (Fig 5A). SIM confirmed that both proteins were in very close proximity (Fig 5B); the same could also be shown for LPS/ATP-treated *Becn1*^{+/-} microglia (Appendix Fig S2B). The colocalization of NLRP3 and CALCOCO2 was confirmed by performing 3D radial intensity profiles on NLRP3 clusters in wild-type (Fig 5C) and *Becn1*^{+/-} microglia (Appendix Fig S2C). To further substantiate this interaction and to investigate the location of both proteins within the autophagosome, we used the SIM images from wild-type microglia and compared the LC3 and CALCOCO2 signal in the center of NLRP3 clusters with its maximal intensity within the cluster. Clearly, the relative center intensity of CALCOCO2 (~95%) was significantly higher than the center intensity of LC3 (~60%) (Fig 5D). These data strongly suggest that NLRP3 interacts with CALCOCO2 within the lumen of autophagosomes, while LC3 is localized to both sides of the autophagosomal membrane.

Murine cells express a truncated form of CALCOCO2 containing the SKICH, LIR, and coiled-coil domain but not the ubiquitin-binding and galectin-8 domains (Tumbarello *et al*, 2015). To determine whether the close localization of murine CALCOCO2 to NLRP3 may have a functional impact and is related to cytokine production, microglia were treated with a CALCOCO2 siRNA, which resulted in significant reduction in the protein (Fig 5E). After LPS/ATP stimulation, cells with CALCOCO2 knockdown released more IL-1beta into the supernatant (Fig 5F), while TNFalpha and IL-6 levels remained unchanged (Fig EV5D and E) compared to microglia transfected with a scrambled siRNA. These data support the idea that CALCOCO2 binds NLRP3 most probably via the SKICH domain (see Discussion) and is involved in the modulation of IL-1beta response.

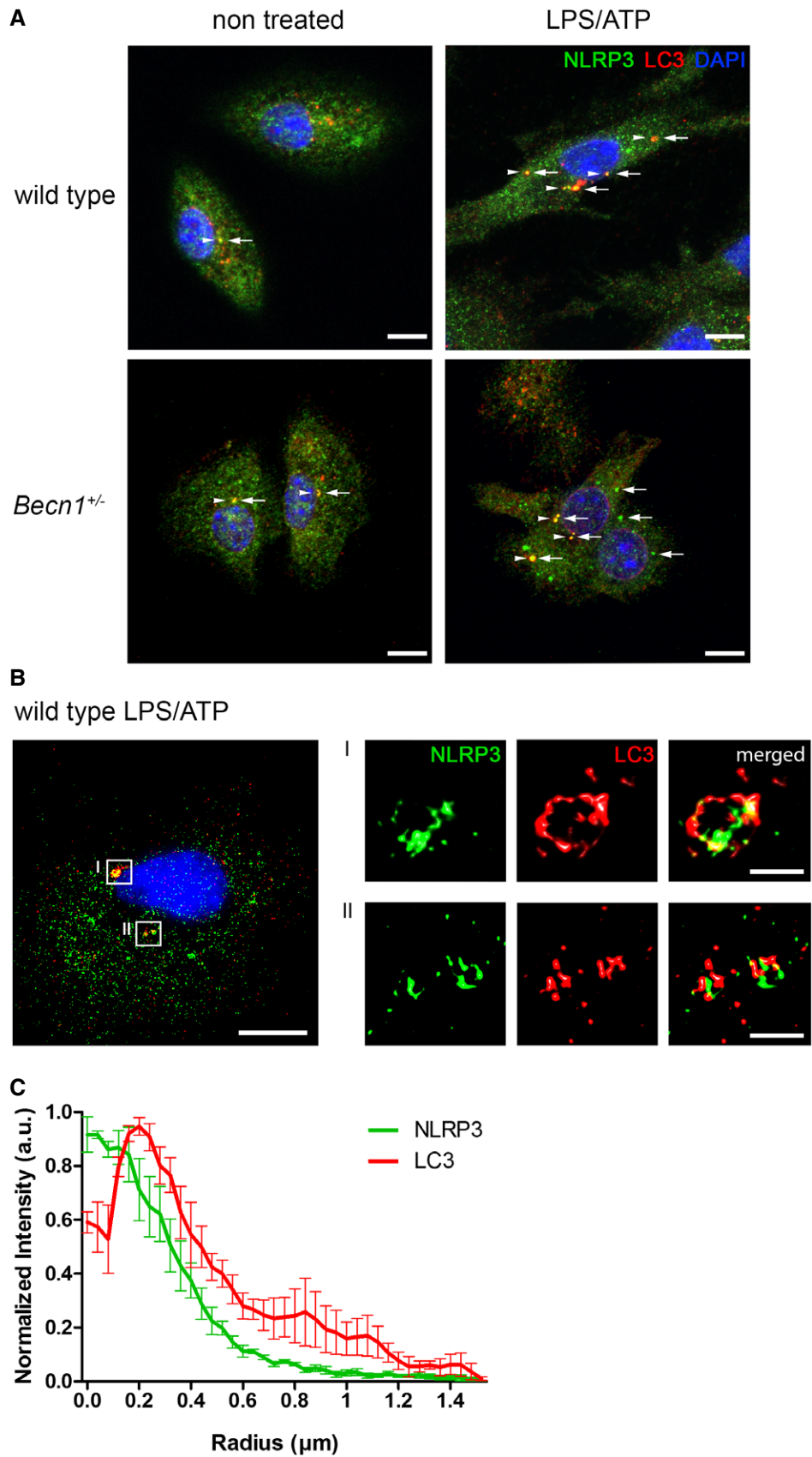


Figure 4.

Figure 5. CALCOCO2/NDP52 colocalizes with NLRP3 and modulates IL-1beta release.

- A LPS/ATP-treated wild-type microglia were stained for NLRP3 (green) and CALCOCO2 (red) and analyzed by confocal microscopy. Colocalizations of NLRP3 aggregates (arrows) and CALCOCO2 (arrowheads) are apparent; scale bar: 10 μ m.
- B LPS/ATP-treated wild-type microglia were stained for NLRP3 (green) and CALCOCO2 (red) and analyzed by super-resolution microscopy (SIM). NLRP3 aggregates coclustering with CALCOCO2-positive signals are visible. 3D volume rendering of NLRP3 aggregates from the magnified ROIs showed close contact of NLRP3 with CALCOCO2; scale bar: 10 μ m; magnified ROIs: 1 μ m.
- C 3D Radial intensity profiles of NLRP3 and CALCOCO2 signals derived from SIM images in wild-type microglia, centered on the maxima of NLRP3 clusters. The radial profiles confirm that both proteins colocalize; mean \pm SEM, $n = 3$.
- D In SIM images from wild-type microglia the subautophagosomal localization of LC3 and CALCOCO2 was analyzed in relation to NLRP3. LC3 and CALCOCO2 intensities at the center of NLRP3 aggregates were normalized to their maximum within the same cluster. While CALCOCO2 intensity is near maximal at the center of NLRP3 aggregates (indicating the luminal localization of CALCOCO2), the relative LC3 intensity was significantly lower (in agreement with the LC3 localization at autophagosomal membranes); LC3: $n = 4$, CALCOCO2: $n = 3$; two-tailed t -test $**P < 0.01$.
- E Microglia from *Becn1*^{+/-} mice were transfected with scrambled siRNA or with siRNA for CALCOCO2. 6 d after transfection, cells were stimulated with LPS/ATP. The expression of CALCOCO2 protein was determined by Western blot. Application of CALCOCO2 siRNA resulted in significantly reduced expression of CALCOCO2; mean \pm SEM, $n = 3$; two-tailed t -test $*P < 0.05$.
- F The amount of IL-1beta in the supernatant released from the cells described in (E) was determined by ELISA. Microglia with a CALCOCO2 knockdown released significantly more IL-1beta; mean \pm SEM, $n = 3$; two-tailed t -test $*P < 0.05$.

Discussion

In this study, we analyzed the effects of reduced BECN1 levels on the inflammatory process in microglia *in vitro* after an acute pro-inflammatory stimulus and *in vivo* in an AD-like mouse model with amyloid-beta pathology and neuroinflammation. Impaired autophagy has been linked to AD in various ways as detailed in recent reviews (Menzies *et al*, 2015, 2017), but research until now has concentrated almost exclusively on neurons. However, neuroinflammation is an important driver of AD (Heppner *et al*, 2015), and since microglia are the main producers of pro-inflammatory cytokines in the brain, they are in the center of interest when investigating neuroinflammation. BECN1 is a key protein of the autophagic pathway, and its reduction in *Becn1*^{+/-} mice resulted accordingly in diminished autophagic flux and autophagosome formation. This is in agreement with reports demonstrating reduced autophagy in neurons, muscle, and endothelial cells isolated from *Becn1*^{+/-} mice (Qu *et al*, 2003; Pickford *et al*, 2008), which further indicates that microglial BECN1 reduction impairs autophagy. *Becn1*^{-/-} microglia could not be employed in this study since *Becn1*^{-/-} embryos die *in utero* very early between E7.5 and E8.5 (Yue *et al*, 2003), thus at a time point before microglia precursors leave the yolk sac to colonize the developing brain (starting at E9.5) (Ginhoux *et al*, 2010; Swinnen *et al*, 2013; Tay *et al*, 2017).

In vitro genetic reduction in *Becn1* or addition of the autophagy blocker 3-MA resulted in increased expression of IL-1beta and IL-18 after addition of a standard acute pro-inflammatory stimulus (LPS followed by ATP), while TNFalpha or IL-6 was not altered. The specific targeting of the IL-1beta/IL-18 pathway by impaired autophagy is in agreement with previous data showing no effect on TNFalpha release after knockdown of *Atg7* in neonatal microglia (Cho *et al*, 2014). In contrast, Ye *et al* (2017) observed not only enhanced IL-1beta levels, but also an increase in TNFalpha and IL-6 after impairment of autophagy by 3-MA, or after knockdown of *Becn1* or *Atg5* in the microglial cell line BV2. Additionally, Santeford *et al* (2016) also described enhanced IL-6 levels after loss of *Atg5*. A recent analysis of microglia from different origins revealed that the expression profile of primary microglia differs from BV2 cells, where neonatal primary microglia resemble adult microglia more closely than BV2 cells, which could account for the different findings (Butovsky *et al*, 2014). Also, macrophages with loss of *Atg16l1*

exhibited a specific increase in IL-1beta/IL-18 production and showed no effect on TNFalpha or IL-6 production (Saitoh *et al*, 2008). Based on these data, we conclude that the observed increase in IL-1beta/IL-18 production in *Becn1*^{+/-} microglia is not caused by a general microglial priming and activation mediated by impaired autophagy, but rather a specific intervention of the IL-1beta/IL-18 processing pathway.

To support this hypothesis, we analyzed whether reduction in BECN1 also increased IL-1beta levels *in vivo* in an Alzheimer-like setting using the established amyloid pathology model *APPSP1* (Radde *et al*, 2006). Production of IL-1beta in microglia occurs *in vivo* only after priming (Perry & Holmes, 2014) and the *Il1b* gene is upregulated in primed microglia of *APPSP1* mice, as well as in acutely LPS-activated microglia as shown in a differential transcriptome analysis (Holtman *et al*, 2015). Heterozygous loss of *Becn1* alone did not result in increased IL-1beta protein levels in the brain compared to age-matched wild-type mice. As the oldest analyzed mice were only 8 months old, an aging-mediated effect had apparently not yet occurred. However, it could be possible that older mice show an impact of *Becn1* heterozygosity, as 24-month-old mice exhibited an upregulation of *Il1b* (Holtman *et al*, 2015).

In support of this hypothesis, we observed a significant age-dependent upregulation of IL-1beta in TBS and TX protein fractions from the brains from 4- and 8-month-old *APPSP1 Becn1*^{+/-} mice. Thus, when microglia were primed by extracellular amyloid-beta, the reduced levels of BECN1 mediated an increase in IL-1beta production. *In vitro*, this was an IL-1beta specific effect, as no changes in TNFalpha were observed. However, the impact of BECN1 reduction on IL-6 remains unclear. While no effect on IL-6 release was observed *in vitro* and *in vivo* in the TBS fraction, an increase in IL-6 in the TX fraction of 8-month-old *APPSP1 Becn1*^{+/-} mice became apparent, warranting further investigation.

In *APPSP1 Becn1*^{+/-} mice, neither changes in the amyloid-beta load were detected nor phagocytosis was altered. On first sight, this appears to be in contrast to data from Pickford *et al* (2008), who observed an increase in amyloid pathology in 9-month-old *T41APP Becn1*^{+/-} mice. However, this difference can be explained by the fact that another transgenic mouse strains were used in our experiments, particularly by the strong impact of the two overexpressed transgenes *APP* and *PS1* in *APPSP1* mice used herein. Knockdown of *Becn1* in BV2 microglial cells has been shown to reduce

A wild type LPS/ATP

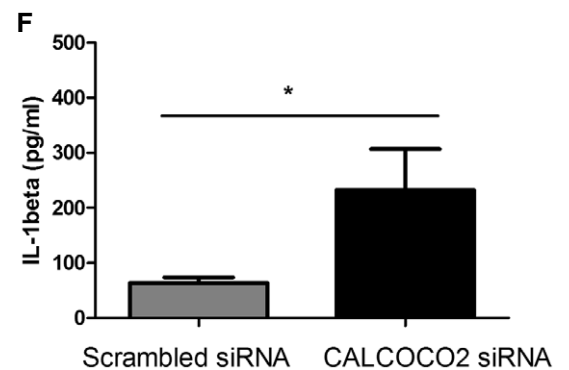
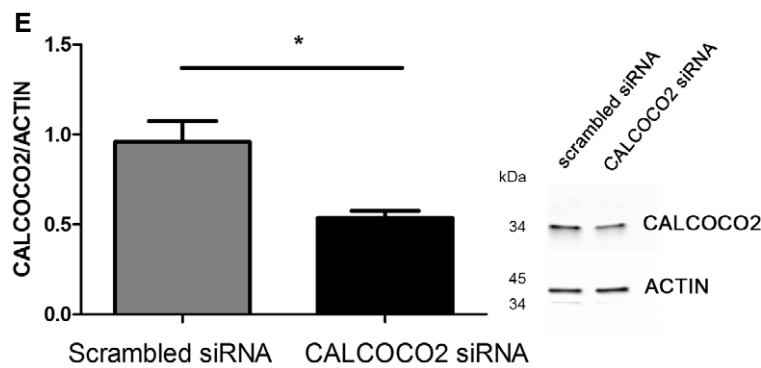
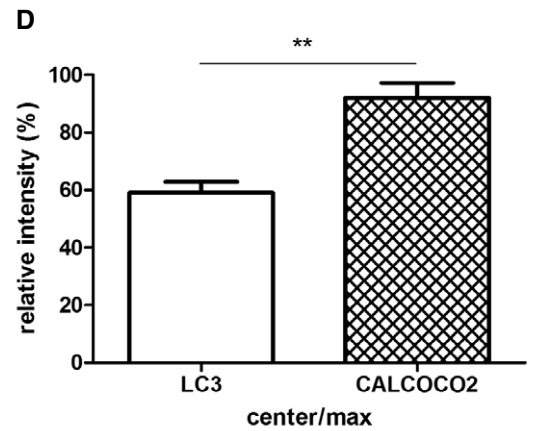
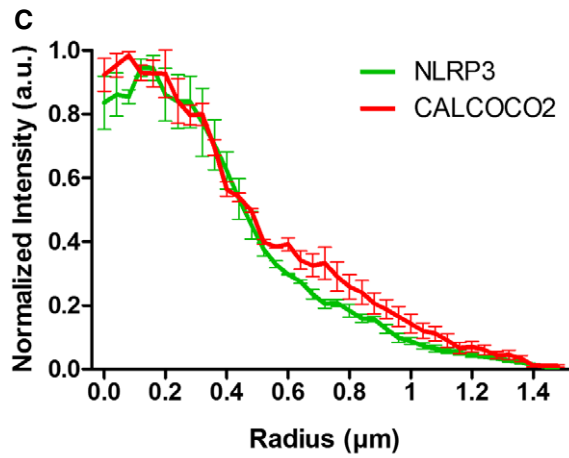
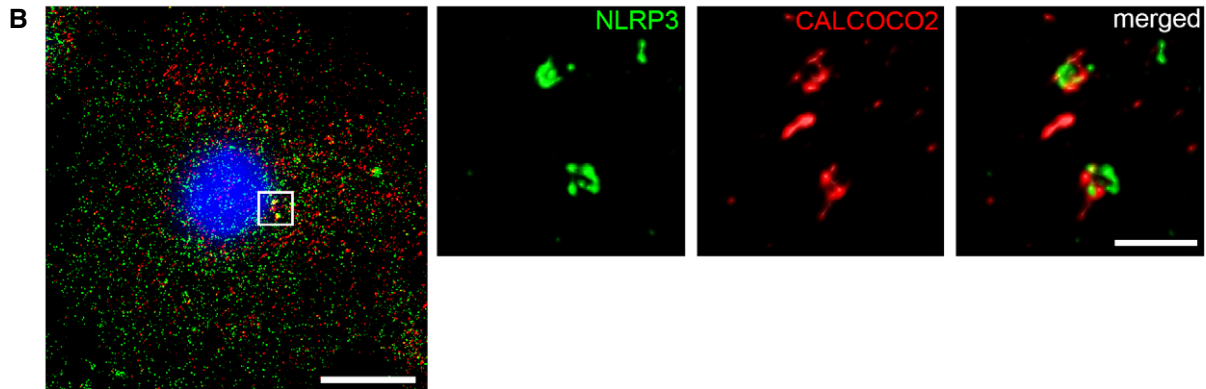
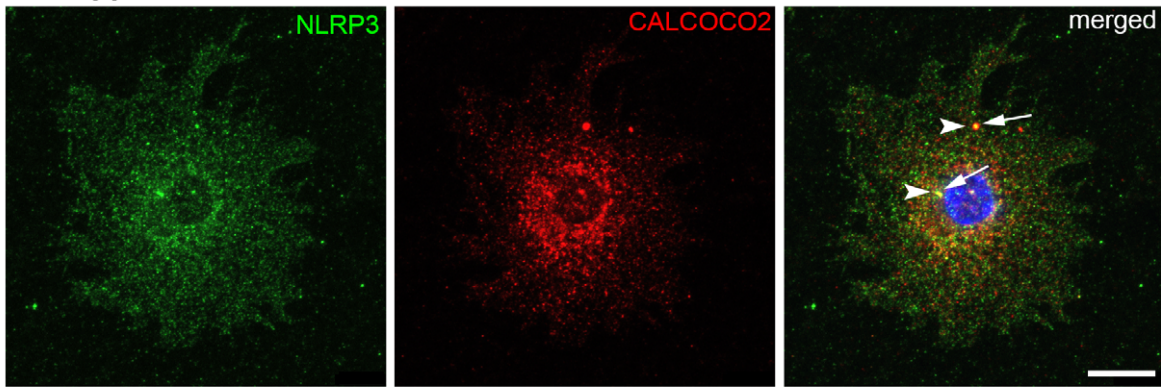


Figure 5.

phagocytosis (Lucin *et al*, 2013), while an increase in IL-1beta expression is supposed to augment the phagocytic activity (Ferreira *et al*, 2011). While the lack of a difference in phagocytosis in *APPPS1 Becn1^{+/-}* microglia certainly explains why there is no substantial difference in amyloid-beta burden in *APPPS1* mice with one versus two alleles of *Becn1*, it appeared to be counter-intuitive at first sight, also in light of previous data showing that IL-1beta release can drive the phagocytic capacity of microglia. However and importantly, Lucin *et al* (2013) demonstrated that knocking down Beclin1 in BV2 microglial cells reduces the phagocytic capacity of these cells. Based on this, we assume that the Beclin1-mediated decrease in phagocytosis, which should also apply to *Becn1^{+/-}* microglia, may be compensated by the IL-1beta-driven reverse effect, that is, that in heterozygous *Becn1^{+/-}* microglia these opposing effects modulating phagocytosis outcompete each other. Along this line, one would speculate that *APPPS1* mice with a homozygous deletion of Beclin1 are expected to harbor microglia with reduced phagocytic microglia, supposedly resulting in an increase in amyloid pathology. The respective experimental *in vivo* proof of this hypothesis is, however, difficult to provide given that homozygous Beclin1 knock-out mice are lethal (Qu *et al*, 2003; Yue *et al*, 2003). Future studies, perhaps with older mice, may answer this question. Alternatively, a microglia-targeted complete loss of BECN1 by using a *Becn1^{flox/flox}* mouse crossed to a *Cx3cr1^{Cre}* or *Sall1^{Cre}* mouse could maximize the effects shown here.

A fundamental question is the mechanism by which reduced BECN1 levels and autophagy modulate the IL-1beta/IL-18 production. Proposed mechanisms include degradation of pro-IL-1beta (Harris *et al*, 2011), degradation of inflammasomes (Shi *et al*, 2012), and an indirect activation of the inflammasome via accumulation of dysfunctional mitochondria and oxidative stress due to impaired mitophagy (Saitoh *et al*, 2008; Zhou *et al*, 2011; Lodder *et al*, 2015; Lee *et al*, 2016; Ye *et al*, 2017). Since no significant changes in pro-IL-1beta levels were observed, we investigated other steps in the IL-1beta/IL-18 processing pathway. Here, increased levels of NLRP3 and cleaved CASP1 alongside a higher percentage of cells with ASC-stained inflammasomes were detected. Pro-CASP1 is cleaved into p10 and p20 fragments, which were reported to be degraded via the ubiquitin-proteasome system (Squires *et al*, 2007; Muehlbauer *et al*, 2010; Van Opdenbosch *et al*, 2014). Therefore, SIM was used as a super-resolution microscopy method to determine the fate of NLRP3 and the inflammasomes. Staining of endogenous NLRP3 in LPS/ATP-stimulated microglia revealed several distinct, highly fluorescent NLRP3 puncta/specs in addition to a rather diffuse cytoplasmic staining, which was also observed in non treated cells. The specificity of the NLRP3 staining was confirmed using SIM by co-staining with ASC: An intimate contact between NLRP3 and ASC in activated cells could be observed. Structurally, this interaction resembled the NLRP3-ASC interaction observed in the *Salmonella*-induced inflammasome (Man *et al*, 2014), where ASC is forming a ring-like scaffold for NLRP3. One apparent difference is the presence of two or more intervened ASC rings in the inflammasome of LSP/ATP-stimulated microglia, which is not seen in *Salmonella*-induced inflammasome activation.

The co-staining of endogenous LC3 and NLRP3 revealed numerous colocalizations of both signals. This correlates with data of Chuang *et al* (2013) that showed colocalization of overexpressed and fluorescence-tagged LC3 and NLRP3 in HEK293 cells.

Stimulated myeloid cells normally contain only one or two ASC-containing inflammasomes (Baroja-Mazo *et al*, 2014; Franklin *et al*, 2014) (see also Fig 3C) that are also significantly larger than most of the NLRP3 signals seen in these cells (see Fig EV4C and D). Murine NLRP3 has a calculated molecular weight of 113 kDa and the pyrin domain has to exist at least as a trimer to trigger IL-1beta production, which is apparently independent of the formation of ASC-containing inflammasome (Susjan *et al*, 2017). Thus, it seems plausible that the observed smaller NLRP3 aggregates present NLRP3 trimers or higher oligomeric forms as suggested for NLRP2 (Faustin *et al*, 2007) or NLRC4 (Hu *et al*, 2015; Zhang *et al*, 2015). The large NLRP3-positive aggregates are likely part of a completely assembled, ASC-containing inflammasome. NLRP3 colocalized with mitochondria as shown before (Zhou *et al*, 2011; Subramanian *et al*, 2013; Bracey *et al*, 2014), whereas we could not observe a colocalization of NLRP3, mitochondria, and LC3, indicating that mitochondria are not involved in the degradation of NLRP3, or that NLRP3 has no substantial impact on mitophagy, respectively.

SIM pictures of small and large NLRP3 aggregates confirmed the localization of NLRP3 to LC3-positive autophagosomes. The described adaptor protein for the autophagic removal of inflammasomes, p62/SQSTM1 (Shi *et al*, 2012), did not colocalize with or bind to NLRP3. In contrast, CALCOCO2 interacted directly with NLRP3 and was located significantly nearer to NLRP3 than LC3 in the SIM images. CALCOCO2 has been shown to be involved in mitophagy (Moore & Holzbaur, 2016) and xenophagy (Verlhac *et al*, 2015) in human cells. Murine cells express only a truncated version of CALCOCO2 and its functionality is under discussion. However, the murine protein still contains the SKICH and LIR domain and several domain-specific knock-out studies in CALCOCO2 showed that the SKICH domain is essential for binding TRIF, TRAF6 (Inomata *et al*, 2012), phosphorylated tau, amyloid-beta (Jo *et al*, 2014), and damaged mitochondria (Furuya *et al*, 2018). The LIR domain specifically binds LC3C on the autophagosomal membrane, which then attracts all other ATG8 orthologues (von Muhlinen *et al*, 2013). Our data show that CALCOCO2 is located between NLRP3 and LC3 in a vesicle resembling the size of an autophagosome. While it appears that murine CALCOCO2 is able to bind NLRP3 via its SKICH domain, it is not yet entirely solved whether it acts as an autophagic adaptor protein by also binding LC3, or whether additional proteins are involved in the degradation process to compensate for the missing ubiquitin-binding domain. However, the downregulation of CALCOCO2 by siRNA in microglia resulted in an increase in IL-1beta expression, while TNFalpha and IL-6 were not affected, implying that murine CALCOCO2, despite its truncation, is involved in regulating IL-1beta production in murine microglia.

Materials and Methods

Mice

APPPS1^{+/-} mice were described before (Radde *et al*, 2006). Male *APPPS1^{+/-}* mice were crossed to female Bl6J mice, and *APPPS1^{+/-}* mice were compared to littermate wild-type controls. *Becn1^{+/-}* mice have also been described before (Qu *et al*, 2003) and were a gift from Tony Wyss-Coray (Stanford University School of Medicine/USA). Mice were bred from heterozygous matings. *Becn1^{+/-}* mice

were compared to littermate wild-type controls. Animals were kept in individually ventilated cages with a 12-h light cycle with food and water *ad libitum*. All animal experiments were conducted in accordance with animal welfare acts and were approved by the regional office for health and social service in Berlin (LaGeSo).

Microglia isolation and culture

Newborn animals (2–4 days) were killed by decapitation. The meninges were removed, and the brain was homogenized. Cells were separated by incubation with 0.1% trypsin for 15 min at 37°C. Cells were cultivated at 37°C with 5% CO₂ and 95% air in DMEM (41966-029, Invitrogen) with 10% FCS (Invitrogen) and 1% penicillin/streptomycin (Invitrogen) for 7 DIV until a confluent glial cell layer (astrocytes and microglia) was formed. To induce microglial proliferation, the mixed glial culture was stimulated from day 7 on with GM-CSF (Miltenyi Biotec, 130-095-746) with a final concentration of 5 ng/ml. Microglia were harvested at DIV 10–14 by 6 min of shaking. Microglial identity was confirmed by immunostaining for Iba1 and CD68.

Adult animals were anesthetized with isoflurane, euthanized by CO₂, and transcardially perfused with 1× PBS. The brain was removed and dissected, followed by homogenizing using the gentle MACS Octo Dissociator (Miltenyi Biotec). Next, magnetic sorting using CD11b+ magnetic beads (Miltenyi Biotec, 130-093-634) was performed. Prior to (i.e., directly after tissue dissociation) and after MACS sorting, isolated cells are stained with CD45 and CD11b antibodies and analyzed by flow cytometry using the expression levels of CD11b and of CD45 to distinguish resident microglia (CD11b+CD45int) from other CNS macrophages (CD11b+CD45hi) including meningeal macrophages or from other (systemic) inflammatory cells such as peripheral leukocytes (CD11b-CD45hi). Only isolations with a purity of 95% of CD11b-positive macrophages/microglia were used for further analysis.

After sorting, the cells were seeded on PLL-coated coverslips, 1 × 10⁶ cells/well, and fixed with ice-cold methanol after 3 h at 37°C. Subsequently, they were stained for LC3 and NLRP3, see Immunocytochemistry section.

Microglia treatment

Microglia from newborn mice were seeded in 24-well plates and incubated overnight in growth medium DMEM (Invitrogen) with 10% FCS (Invitrogen) and 1% penicillin/streptomycin (Invitrogen) without GM-CSF. Next day, cells were kept for 2 h in growth medium or HBSS as indicated. As a pro-inflammatory stimulus, LPS (final concentration 1 µg/ml) for 3 h followed by ATP (final concentration 1 mM) for 45 min was used before supernatant and cells were harvested. 3-MA (Sigma-Aldrich, M9282, final concentration 10 mM) was added 1 h 45 min before the end of the experiment. To measure autophagic flux, microglia were kept for 2 h in cultivation medium or HBSS (24020-091, Invitrogen) in the presence of Bafilomycin A1 (Sigma-Aldrich, B1793, final concentration 5 nM).

siRNA transfection

Microglia were seeded as described above. Next day, medium was exchanged and cells were transfected with a complex of Viromer Blue (Lipocalyx, VB-01LB-00) and CALCOCO2 FlexiTube siRNA #4

(Qiagen, 1027416/GS76815), according to manufacturer's instruction. Every 2 days, fresh medium was added to the wells. Six days after transfection, cells were stimulated with LPS/ATP as described above.

ELISA

The supernatant of stimulated microglia was diluted 1:10–1:20 or used undiluted (IL-18). IL-1beta (eBioscience, 88701388), IL-18 (MBL, MBL-7625), TNFalpha (eBioscience, 88723477), and IL-6 (eBioscience, 88706488) concentration was determined according to the manufacturer's instructions.

The cytokine content as well as the amyloid-beta burden of the whole brain was determined using a MESO QuickPlex SQ 120 system (Meso Scale Discovery) and the V-PLEX Pro-inflammatory Panel 1 (Meso Scale Discovery, K15048D1) and the V-PLEX Aβ Peptide Panel 1 (4G8) (Meso Scale Discovery, K15199E), respectively. Proteins were extracted from mouse brains using the four-step protocol as described before (Kawarabayashi *et al*, 2001). The TBS fraction and the Triton-X fraction containing the soluble proteins were measured without further dilution. The SDS fraction was diluted 1:500 prior to measuring insoluble proteins.

Western blotting

Protein lysates were separated by SDS-PAGE using (depending on size) a Tris–Glycine or a Tris–Tricine buffer system and transferred by wet blotting onto a nitrocellulose membrane. The following antibodies were used: BECN1 (Novus, NB500-249 or Cell Signaling, 3495), LC3 (Sigma, L8918), CASP1 and pro-CASP1 (Abcam, ab179515), IL-1beta and pro-IL-1beta (eBioscience, 88701388), NLRP3 (AdipoGen, AG-20B-0014), p62/SQSTM1 (MBL, PM045), CALCOCO2 (Abiocode, R2269-1), and ACTIN (Sigma, A1978). For visualization of the bands, the SuperSignal[®] West Femto Chemiluminescent Substrate (Thermo, 34096) for detection of horseradish peroxidase activity was used. The quantification of the respective intensities of all bands was achieved with the program ImageJ, and the amount of the respective protein was normalized to the ACTIN protein content.

Phagocytosis assay in acute brain slices

The assay was performed as described before (Krabbe *et al*, 2013). In brief, mice were decapitated and brains were carefully removed and washed in carbogen-saturated artificial cerebrospinal fluid (aCSF), pH 7.4. 130-µm-thick coronal slices were prepared using a vibratome (Microm, Walldorf, Germany) at 4°C and were kept in brain slice buffer at room temperature (21–25°C) for 2 h. The acute brain slices were then incubated with a suspension of FCS-coated yellow-green fluorescent carboxylated microspheres (2 µm diameter, Polysciences Europe GmbH) at a concentration of 1.7 × 10⁷ microspheres/ml for 60 min at 37°C, extensively washed, and finally fixed with 4% paraformaldehyde. Brain sections were stained with anti-Iba1 (Wako, 019-19741) antibody to visualize microglia.

Phagocytosis assay analysis

In brain sections derived from acute brain slices, z-stacks of 20 µm thickness were produced using a 40× objective with a step size of 1 µm beginning at the top of the slice, where the microspheres are

located. Beads per cell were counted using ImageJ cell counter plugin ensuring that only beads inside a cell were counted as positive. The phagocytic index was determined by assessing the percentage of cells, which contained 0, 1–4, 5–7, 8–10, and > 10 microspheres per cell. The percentage of cells in each group was multiplied by the corresponding grade of phagocytosis (1–4:1, 5–7:2, 8–10:3, > 10:4). The sum of the products in each group was then termed and displayed as phagocytic index (Krabbe *et al*, 2013). Six ROIs (i.e., fields of view) were analyzed per animal.

Histology

Formalin-fixed and sucrose-treated brain hemispheres were frozen and cryosectioned coronally at 30 μm . Tissue sections were collected throughout the entire rostrocaudal extent of the brain and stored at 4°C until staining. Immunohistochemistry and subsequent stereological analyses were performed on 10–12 systematically randomly sampled sections collected at 180- μm intervals for each marker analyzed. Free-floating sections were stained for microglia with the antibody Iba1 (1:500, Wako, 019-19741) or for amyloid-beta using the antibody 4G8 (1:500, Covance, Sig39220-500). Core plaques were stained with Congo red (Carl Roth).

Stereology

Stereology was performed using a Stereo Investigator system (MicroBrightField) and DV-47d camera (MicroBrightField) mounted on a BX53 microscope (Olympus). Stereological quantification of Iba1+ cells and Congo red+ plaques was performed using the optical fractionator method (MicroBrightField). Quantification of 4G8+ plaques was performed using the area fractionator method (MicroBrightField).

Immunocytochemistry

Co-staining of NLRP3 with LC3, p62, mitochondria, or CALCOCO2

Microglia were cultured overnight on Poly-L-Lysine-coated coverslips. For visualization of mitochondria, cells were incubated for 1 h with MitoTracker Red CMX ROS (MTR; Thermo Fisher # M7512) (final concentration 25 nM) prior to stimulation. Autophagosomes were stained according to Kistakis (Kistakis, 2015). Shortly, cells were fixed with ice-cold methanol for 10 min and blocked overnight in 1 \times PBS with 2% bovine serum albumin. LC3 antibody (Sigma, L7543), p62 (Santa Cruz, sc-25575), respectively, and CALCOCO2 antibody (Proteintech, 12229-1-AP) were added for 1 h (1:200), followed by an Alexa568-conjugated secondary antibody (Invitrogen, 11011) for 1 h (1:500). Afterward, the NLRP3 antibody (AdipoGen, AG-20B-0014) was added overnight (1:500), followed by an Alexa488-conjugated secondary antibody (Invitrogen, 11001) for 1 h (1:500).

ASC

Microglia were cultured overnight on Poly-L-Lysine-coated coverslips, fixed with 4% paraformaldehyde for 20 min, permeabilized with 0.1% Triton X-100 for 20 min, blocked with 3% bovine serum albumin for 1–3 h in 1 \times PBS, and incubated overnight in PBS with the primary antibody ASC (AdipoGen, AG-25B-0006, 1:500). Next day, incubation with an Alexa568-conjugated secondary antibody (Invitrogen, 11011) was performed for 1 h.

Nuclei were counterstained with DAPI (Roche, 10236276001). Samples were mounted with Fluorescent Mounting Medium (Dako, S3023).

Microscopy

Confocal laser scanning microscopy

A Leica TCS SP5 confocal laser scanning microscope controlled by LAS AF scan software (Leica Microsystems, Wetzlar, Germany) was used. Images were taken simultaneously and assembled to stacks. LC3-positive vesicles, NLRP3 aggregates, and ASC specks were counted with the program ImageJ and normalized on the cell area (without the nuclear area), respectively, the cell number. Images in the figures represent maximum image projections.

SIM

3D 3-color SIM images were acquired using the 405, 488, and 568 nm laser lines, standard filter sets, and 125 nm z-sectioning of the OMX V4 Blaze (GE Healthcare) system. 100-nm fluorescent beads (TetraSpeck, T7284, Thermo Fisher Scientific) were used for registration of the detection channels, achieving < 40 nm registration error for all three channels. 3D-rendering, image and movie export was done with Arivis Vision4D and ImageJ (Schneider *et al*, 2012).

Image analysis of SIM pictures

The centers (center of mass) of NLRP3 clusters or dapi-stained nuclei were determined in SIM images with Arivis Vision4D using a histogram-based threshold procedure (Otsu's method). NLRP3 clusters were additionally filtered with a size exclusion filter against small objects (minimal diameter 500 nm). 3D radial intensity profiles around cluster centers were generated with a custom-written ImageJ macro (Schneider *et al*, 2012). Averaged intensity values were plotted against their radial distance to the center of mass of single clusters in the reference channel (NLRP3). Distances between NLRP3 clusters and the nucleus were calculated based on the segmentation objects using a custom-written Python script.

Data analysis

Values are presented as mean \pm SEM (standard error of the mean). Statistical difference between means was assessed either by the two-tailed *t*-test for two groups or ANOVA with the indicated *post hoc* test for more than two groups using the GraphPad Prism software. Statistically significant values are indicated by **P* < 0.05, ***P* < 0.01, and ****P* < 0.001.

Expanded View for this article is available online.

Acknowledgements

We are very grateful for the donation of the *Becn1*^{+/-} mice from Tony Wyss-Coray (Stanford University School of Medicine/USA) and intriguing discussions. We thank Aniki Knop and Sebastian Dumkow for excellent technical support. We are indebted to Paul Mohr for support in designing the synopsis image. We would also like to thank Annisa Chand for critical proofreading of the manuscript. This work was supported by the Deutsche Forschungsgemeinschaft (SFB TRR 43, SFB TRR 167, NeuroCure Exc 257, and HE 3130/6-1 to FLH; DFG grant JE278/6-1 to MJ), by the Berlin Institute of Health (BIH; Collaborative Research Grant to FLH), and by the European Union (PHAGO; Innovative

Medicines Initiative-2). The work of N.G. was supported by the DFG SFB958/202 to J.S and the Advanced Medical Bioimaging Core Facility (AMBIO) of the Charité—Universitätsmedizin.

Author contributions

JH, KF, and MJ performed the experimental work and analysis. NG and JS were responsible for the super-resolution microscopy and analysis. MJ and FLH designed the experiments. All authors wrote, revised, and approved the manuscript.

Conflict of interest

The authors declare that they have no conflict of interest.

References

- Baroja-Mazo A, Martin-Sanchez F, Gomez AI, Martinez CM, Amores-Iniesta J, Compan V, Barbera-Cremades M, Yague J, Ruiz-Ortiz E, Anton J, Bujan S, Couillin I, Brough D, Arostegui JJ, Pelegrin P (2014) The NLRP3 inflammasome is released as a particulate danger signal that amplifies the inflammatory response. *Nat Immunol* 15: 738–748
- Bracey NA, Gershkovich B, Chun J, Vilaysane A, Meijndert HC, Wright JR Jr, Fedak PW, Beck PL, Muruve DA, Duff HJ (2014) Mitochondrial NLRP3 protein induces reactive oxygen species to promote Smad protein signaling and fibrosis independent from the inflammasome. *J Biol Chem* 289: 19571–19584
- Butovsky O, Jedrychowski MP, Moore CS, Cialic R, Lanser AJ, Gabriely G, Koeglsperger T, Dake B, Wu PM, Doykan CE, Fanek Z, Liu L, Chen Z, Rothstein JD, Ransohoff RM, Cygi SP, Antel JP, Weiner HL (2014) Identification of a unique TGF- β -dependent molecular and functional signature in microglia. *Nat Neurosci* 17: 131–143
- Cho M-H, Cho K, Kang H-J, Jeon E-Y, Kim H-S, Kwon H-J, Kim H-M, Kim D-H, Yoon S-Y (2014) Autophagy in microglia degrades extracellular β -amyloid fibrils and regulates the NLRP3 inflammasome. *Autophagy* 10: 1761–1775
- Chuang SY, Yang CH, Chou CC, Chiang YP, Chuang TH, Hsu LC (2013) TLR-induced PAI-2 expression suppresses IL-1 β processing via increasing autophagy and NLRP3 degradation. *Proc Natl Acad Sci USA* 110: 16079–16084
- Faustin B, Lartigue L, Bruet JM, Luciano F, Sergienko E, Bailly-Maitre B, Volkmann N, Hanein D, Rouiller I, Reed JC (2007) Reconstituted NALP1 inflammasome reveals two-step mechanism of caspase-1 activation. *Mol Cell* 25: 713–724
- Ferreira R, Santos T, Viegas M, Cortes L, Bernardino L, Vieira OV, Malva JO (2011) Neuropeptide Y inhibits interleukin-1 β -induced phagocytosis by microglial cells. *J Neuroinflammation* 8: 169
- Fillit H, Ding W, Buee L, Kalman J, Altstiel L, Lawlor B, Wolf-Klein G (1991) Elevated circulating tumor necrosis factor levels in Alzheimer's disease. *Neurosci Lett* 129: 318–320
- François A, Terro F, Janet T, Bilan A, Paccalin M, Page G (2013) Involvement of interleukin-1 β in the autophagic process of microglia: relevance to Alzheimer's disease. *J Neuroinflammation* 10: 1–22
- Franklin BS, Bossaller L, De Nardo D, Ratter JM, Stutz A, Engels G, Brenker C, Nordhoff M, Mirandola SR, Al-Amoudi A, Mangan MS, Zimmer S, Monks BG, Fricke M, Schmidt RE, Espevik T, Jones B, Jarnicki AG, Hansbro PM, Busto P et al (2014) The adaptor ASC has extracellular and “prionoid” activities that propagate inflammation. *Nat Immunol* 15: 727–737
- Furuya N, Kakuta S, Sumiyoshi K, Ando M, Nonaka R, Suzuki A, Kazuno S, Saiki S, Hattori N (2018) NDP52 interacts with mitochondrial RNA poly(A) polymerase to promote mitophagy. *EMBO Rep* 19: e46363
- Ginhoux F, Greter M, Leboeuf M, Nandi S, See P, Gokhan S, Mehler MF, Conway SJ, Ng LG, Stanley ER, Samokhvalov IM, Merad M (2010) Fate mapping analysis reveals that adult microglia derive from primitive macrophages. *Science* 330: 841–845
- Griffin WS, Stanley LC, Ling C, White L, MacLeod V, Perrot LJ, White CL, Araoz C (1989) Brain interleukin 1 and S-100 immunoreactivity are elevated in Down syndrome and Alzheimer disease. *Proc Natl Acad Sci USA* 86: 7611–7615
- Harris J, Hartman M, Roche C, Zeng SG, O'Shea A, Sharp FA, Lambe EM, Creagh EM, Golenbock DT, Tschopp J, Kornfeld H, Fitzgerald KA, Lavelle EC (2011) Autophagy controls IL-1 β secretion by targeting Pro-IL-1 β for degradation. *J Biol Chem* 286: 9587–9597
- Heneka MT, Kummer MP, Stutz A, Delekate A, Schwartz S, Vieira-Saecker A, Griep A, Axt D, Remus A, Tzeng T-C, Gelpi E, Halle A, Korte M, Latz E, Golenbock DT (2013) NLRP3 is activated in Alzheimer's disease and contributes to pathology in APP/PS1 mice. *Nature* 493: 674–678
- Heppner FL, Ransohoff RM, Becher B (2015) Immune attack: the role of inflammation in Alzheimer disease. *Nat Rev Neurosci* 16: 358–372
- Holtman IR, Raj DD, Miller JA, Schaafsma W, Yin Z, Brouwer N, Wes PD, Moller T, Orre M, Kamphuis W, Hol EM, Boddeke EW, Eggen BJ (2015) Induction of a common microglia gene expression signature by aging and neurodegenerative conditions: a co-expression meta-analysis. *Acta Neuropathol Commun* 3: 31
- Hu Z, Zhou Q, Zhang C, Fan S, Cheng W, Zhao Y, Shao F, Wang HW, Sui SF, Chai J (2015) Structural and biochemical basis for induced self-propagation of NLRC4. *Science* 350: 399–404
- Inomata M, Niida S, Shibata K, Into T (2012) Regulation of Toll-like receptor signaling by NDP52-mediated selective autophagy is normally inactivated by A20. *Cell Mol Life Sci* 69: 963–979
- Jo C, Gundemir S, Pritchard S, Jin YN, Rahman I, Johnson GVW (2014) Nrf2 reduces levels of phosphorylated tau protein by inducing autophagy adaptor protein NDP52. *Nat Commun* 5: 3496
- Kawarabayashi T, Younkin LH, Saido TC, Shoji M, Ashe KH, Younkin SG (2001) Age-dependent changes in brain, CSF, and plasma amyloid (beta) protein in the Tg2576 transgenic mouse model of Alzheimer's disease. *J Neurosci* 21: 372–381
- Krabbe G, Halle A, Matyash V, Rinnenthal JL, Eom GD, Bernhardt U, Miller KR, Prokop S, Kettenmann H, Heppner FL (2013) Functional impairment of microglia coincides with beta-amyloid deposition in mice with Alzheimer-like pathology. *PLoS ONE* 8: e60921
- Krstic D, Madhusudan A, Doehner J, Vogel P, Notter T, Imhof C, Manalastas A, Hilfiker M, Pfister S, Schwerdel C, Riether C, Meyer U, Knuesel I (2012) Systemic immune challenges trigger and drive Alzheimer-like neuropathology in mice. *J Neuroinflammation* 9: 151–151
- Ktistakis NT (2015) Monitoring the localization of MAP1LC3B by indirect immunofluorescence. *Cold Spring Harb Protoc* 2015: 751–755
- Lee HY, Kim J, Quan W, Lee JC, Kim MS, Kim SH, Bae JW, Hur KY, Lee MS (2016) Autophagy deficiency in myeloid cells increases susceptibility to obesity-induced diabetes and experimental colitis. *Autophagy* 12: 1390–1403
- Lodder J, Denaes T, Chobert MN, Wan J, El-Benna J, Pawlowsky JM, Lotersztajn S, Teixeira-Clerc F (2015) Macrophage autophagy protects against liver fibrosis in mice. *Autophagy* 11: 1280–1292
- de Luca A, Smeekens SP, Casagrande A, Iannitti R, Conway KL, Gresnigt MS, Begun J, Plantinga TS, Joosten LAB, van der Meer JWM, Chamilos G, Netea MG, Xavier RJ, Dinarello CA, Romani L, van de Veerdonk FL (2014) IL-1 receptor blockade restores autophagy and reduces inflammation in chronic granulomatous disease in mice and in humans. *Proc Natl Acad Sci USA* 111: 3526–3531
- Lucin KM, O'Brien CE, Czirr E, Mosher KI, Abbey RJ, Mastroeni DF, Rogers J, Spencer B, Masliah E, Wyss-Coray T (2013) Microglial beclin 1 regulates retromer trafficking and phagocytosis and is impaired in Alzheimer's disease. *Neuron* 79: 873–886

- Man SM, Hopkins LJ, Nugent E, Cox S, Gluck IM, Tourlomis P, Wright JA, Cicuta P, Monie TP, Bryant CE (2014) Inflammasome activation causes dual recruitment of NLRC4 and NLRP3 to the same macromolecular complex. *Proc Natl Acad Sci USA* 111: 7403–7408
- Menzies FM, Fleming A, Rubinsztein DC (2015) Compromised autophagy and neurodegenerative diseases. *Nat Rev Neurosci* 16: 345–357
- Menzies FM, Fleming A, Caricasole A, Bento CF, Andrews SP, Ashkenazi A, Fullgrabe J, Jackson A, Jimenez Sanchez M, Karabiyik C, Licitra F, Lopez Ramirez A, Pavel M, Puri C, Renna M, Ricketts T, Schlotawa L, Vicinanza M, Won H, Zhu Y et al (2017) Autophagy and neurodegeneration: pathogenic mechanisms and therapeutic opportunities. *Neuron* 93: 1015–1034
- Mizushima N, Ohsumi Y, Yoshimori T (2002) Autophagosome formation in mammalian cells. *Cell Struct Funct* 27: 421–429
- Moore AS, Holzbaur EL (2016) Spatiotemporal dynamics of autophagy receptors in selective mitophagy. *Autophagy* 12: 1956–1957
- Muehlbauer SM, Lima H Jr, Goldman DL, Jacobson LS, Rivera J, Goldberg MF, Palladino MA, Casadevall A, Brojatsch J (2010) Proteasome inhibitors prevent caspase-1-mediated disease in rodents challenged with anthrax lethal toxin. *Am J Pathol* 177: 735–743
- von Muhlinen N, Akutsu M, Ravenhill BJ, Foeglein A, Bloor S, Rutherford TJ, Freund SM, Komander D, Randow F (2013) An essential role for the ATG8 ortholog LC3C in antibacterial autophagy. *Autophagy* 9: 784–786
- Murthy A, Li Y, Peng I, Reichelt M, Katakam AK, Noubade R, Roose-Girma M, DeVoss J, Diehl L, Graham RR, van Lookeren Campagne M (2014) A Crohn's disease variant in Atg16L1 enhances its degradation by caspase 3. *Nature* 506: 456–462
- Patel NS, Paris D, Mathura V, Quadros AN, Crawford FC, Mullan MJ (2005) Inflammatory cytokine levels correlate with amyloid load in transgenic mouse models of Alzheimer's disease. *J Neuroinflammation* 2: 9–9
- Perry VH, Holmes C (2014) Microglial priming in neurodegenerative disease. *Nat Rev Neurosci* 10: 217–224
- Pickford F, Masliah E, Britschgi M, Lucin K, Narasimhan R, Jaeger PA, Small S, Spencer B, Rockenstein E, Levine B, Wyss-Coray T (2008) The autophagy-related protein beclin 1 shows reduced expression in early Alzheimer disease and regulates amyloid β accumulation in mice. *J Clin Invest* 118: 2190–2199
- Prokop S, Miller KR, Heppner FL (2013) Microglia actions in Alzheimer's disease. *Acta Neuropathol* 126: 461–477
- Qu X, Yu J, Bhagat G, Furuya N, Hibshoosh H, Troxel A, Rosen J, Eskelinen EL, Mizushima N, Ohsumi Y, Cattoretti G, Levine B (2003) Promotion of tumorigenesis by heterozygous disruption of the beclin 1 autophagy gene. *J Clin Invest* 112: 1809–1820
- Radde R, Bolmont T, Kaeser SA, Coomaraswamy J, Lindau D, Stoltz L, Calhoun ME, Jaggi F, Wolburg H, Gengler S, Haass C, Ghetti B, Czech C, Holscher C, Mathews PM, Jucker M (2006) Abeta42-driven cerebral amyloidosis in transgenic mice reveals early and robust pathology. *EMBO Rep* 7: 940–946
- Saitoh T, Fujita N, Jang MH, Uematsu S, Yang BG, Satoh T, Omori H, Noda T, Yamamoto N, Komatsu M, Tanaka K, Kawai T, Tsujimura T, Takeuchi O, Yoshimori T, Akira S (2008) Loss of the autophagy protein Atg16L1 enhances endotoxin-induced IL-1 β production. *Nature* 456: 264–268
- Santeford A, Wiley LA, Park S, Bamba S, Nakamura R, Gdoura A, Ferguson TA, Rao PK, Guan JL, Saitoh T, Akira S, Xavier R, Virgin HWT, Apte RS (2016) Impaired autophagy in macrophages promotes inflammatory eye disease. *Autophagy* 12: 1876–1885
- Schneider CA, Rasband WS, Eliceiri KW (2012) NIH Image to ImageJ: 25 years of image analysis. *Nat Methods* 9: 671–675
- Shi CS, Shenderov K, Huang NN, Kabat J, Abu-Asab M, Fitzgerald KA, Sher A, Kehrl JH (2012) Activation of autophagy by inflammatory signals limits IL-1 β production by targeting ubiquitinated inflammasomes for destruction. *Nat Immunol* 13: 255–263
- Squires RC, Muehlbauer SM, Brojatsch J (2007) Proteasomes control caspase-1 activation in anthrax lethal toxin-mediated cell killing. *J Biol Chem* 282: 34260–34267
- Subramanian N, Natarajan K, Clatworthy MR, Wang Z, Germain RN (2013) The adaptor MAVS promotes NLRP3 mitochondrial localization and inflammasome activation. *Cell* 153: 348–361
- Susjan P, Roskar S, Hafner-Bratkovic I (2017) The mechanism of NLRP3 inflammasome initiation: trimerization but not dimerization of the NLRP3 pyrin domain induces robust activation of IL-1 β . *Biochem Biophys Res Comm* 483: 823–828
- Swinnen N, Smolders S, Avila A, Notelaers K, Paesen R, Ameloot M, Brone B, Legendre P, Rigo JM (2013) Complex invasion pattern of the cerebral cortex by microglial cells during development of the mouse embryo. *Glia* 61: 150–163
- Tay TL, Savage JC, Hui CW, Bisht K, Tremblay ME (2017) Microglia across the lifespan: from origin to function in brain development, plasticity and cognition. *J Physiol* 595: 1929–1945
- Tumbarello DA, Manna PT, Allen M, Bycroft M, Arden SD, Kendrick-Jones J, Buss F (2015) The autophagy receptor TAX1BP1 and the molecular motor myosin VI are required for clearance of salmonella typhimurium by autophagy. *PLoS Pathog* 11: e1005174
- Ulland TK, Song WM, Huang SC, Ulrich JD, Sergushichev A, Beatty WL, Loboda AA, Zhou Y, Cairns NJ, Kambal A, Logvincheva E, Gilfillan S, Cella M, Virgin HW, Unanue ER, Wang Y, Artyomov MN, Holtzman DM, Colonna M (2017) TREM2 maintains microglial metabolic fitness in Alzheimer's disease. *Cell* 170: 649–663.e613
- Van Oudenbosch N, Gurung P, Vande Walle L, Fossoul A, Kanneganti TD, Lamkanfi M (2014) Activation of the NLRP1b inflammasome independently of ASC-mediated caspase-1 autoproteolysis and speck formation. *Nat Commun* 5: 3209
- Verlhac P, Viret C, Faure M (2015) Dual function of CALCO2/NDP52 during xenophagy. *Autophagy* 11: 965–966
- Vom Berg J, Prokop S, Miller KR, Obst J, Kalin RE, Lopategui-Cabezas I, Wegner A, Mair F, Schipke CG, Peters O, Winter Y, Becher B, Heppner FL (2012) Inhibition of IL-12/IL-23 signaling reduces Alzheimer's disease-like pathology and cognitive decline. *Nat Med* 18: 1812–1819
- Walsh JC, Muruve DA, Power C (2014) Inflammasomes in the CNS. *Nat Rev Neurosci* 15: 84–97
- Wang D, Zhang J, Jiang W, Cao Z, Zhao F, Cai T, Aschner M, Luo W (2017) The role of NLRP3-CASP1 in inflammasome-mediated neuroinflammation and autophagy dysfunction in manganese-induced, hippocampal-dependent impairment of learning and memory ability. *Autophagy* 13: 914–927
- Ye J, Jiang Z, Chen X, Liu M, Li J, Liu N (2017) The role of autophagy in pro-inflammatory responses of microglia activation via mitochondrial reactive oxygen species *in vitro*. *J Neurochem* 142: 215–230
- Yue Z, Jin S, Yang C, Levine AJ, Heintz N (2003) Beclin 1, an autophagy gene essential for early embryonic development, is a haploinsufficient tumor suppressor. *Proc Natl Acad Sci USA* 100: 15077–15082
- Zhang L, Chen S, Ruan J, Wu J, Tong AB, Yin Q, Li Y, David L, Lu A, Wang WL, Marks C, Ouyang Q, Zhang X, Mao Y, Wu H (2015) Cryo-EM structure of the activated NAIP2-NLRC4 inflammasome reveals nucleated polymerization. *Science* 350: 404–409
- Zhang D, Wang W, Sun X, Xu D, Wang C, Zhang Q, Wang H, Luo W, Chen Y, Chen H, Liu Z (2016) AMPK regulates autophagy by phosphorylating BECN1 at threonine 388. *Autophagy* 12: 1447–1459
- Zhou R, Yazdi AS, Menu P, Tschopp J (2011) A role for mitochondria in NLRP3 inflammasome activation. *Nature* 469: 221–225